THE JOURNAL OF PHYSICAL CHEMISTRY A
A JOURNAL OF THE AMERICAN CHEMICAL SOCIETY

pubs.acs.org/JPCA

Article

Near-Infrared Spectra of High-Density Crystalline H_2O Ices II, IV, V, VI, IX, and XII

Christina M. Tonauer, Eva-Maria Köck, Tobias M. Gasser, Violeta Fuentes-Landete, Raphael Henn, Sophia Mayr, Christian G. Kirchler, Christian W. Huck, and Thomas Loerting*

Cite This: https://dx.doi.org/10.1021/acs.jpca.0c09764

Read Online

ACCESS | Metrics & More | Article Recommendations | Supporting Information

ABSTRACT: High-pressure ice polymorphs are important for our understanding of hydrogen bonding and exist in the interior of the earth and icy moons. Nonetheless, spectroscopic information about them is scarce, where no information about their optical properties in the near-infrared (NIR) region is available at all. We here report NIR spectra of six ice polymorphs differing in terms of their density and O-atom topology, namely, ices II, IV, V, VI, IX, and XII, in comparison with the known spectra of ice I_h. By contrast to earlier work, we do not use mulling agents or transmission of thin films but use diffuse reflectance on powdered samples in liquid nitrogen. The first overtone of the OH-stretching mode is identified as the marker band most suitable to distinguish between these ices. There is a clear blue shift of this band that increases with increasing topological density in addition to a significant narrowing of the band.

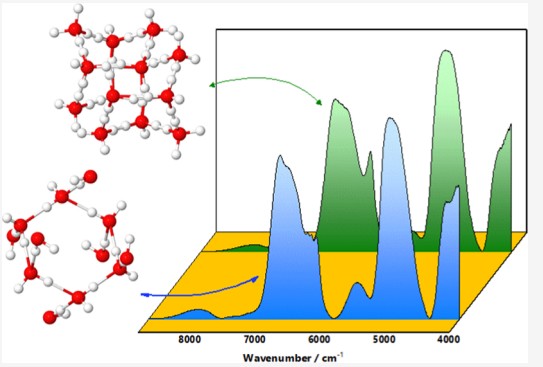

INTRODUCTION

Water exhibits a fascinating range of solid phases termed ices. Hexagonal ice (ice I_h) is the most well-known form, appearing naturally on earth's surface and in ice clouds. The first high-pressure ice polymorphs, ices II and III, were discovered more than 100 years ago by Tammann in the pressure range up to 0.4 GPa.[1−4] Extending the pressure range to 2 GPa, Bridgman discovered ices V and VI in the year 1912.[5] Ice IV appeared as a "ghostly form of ice,"[6] hard to make in a reproducible fashion, and so, it was assigned only in 1935.[7] Such ices do not occur naturally on earth's crust since pressures in the interior of ice sheets and glaciers on the earth do not suffice to transform ice I_h to high-pressure polymorphs. Ice VI and ice VII do exist in earth's mantle, though, as inclusions in superdeep diamonds,[8,9] formed in the mantle's transition zone at depths of 410−660 km.[10] High-pressure ices also exist in the icy mantles of many moons in the Solar System.[11] They might also be present on the surface of icy bodies, such as the Jovian icy moons, through impact events or through transport from the interior to the surface. Once produced, they remain metastable for long times, provided the temperature remains below 150 K.

While all ice polymorphs have been characterized in terms of their crystal structures based on X-ray and/or neutron powder diffraction, spectroscopic information about ice phases is scarce. Only hexagonal ice is reasonably well characterized from the ultraviolet to the microwave part of the electromagnetic spectrum.[12,13] For high-pressure phases, barely any spectroscopic information is available, except for far- and mid-infrared spectra recorded by Whalley and co-workers in the 1960s.[14−17] Raman spectra were recorded by Minčeva-Šukarova and co-workers in the 1980s on ices II, III/IX, V, and VI[18,19] and by Mayer and co-workers in the early 2000s on ices IV,[20] XII/XIV,[21,22] and XIII.[23] Lately, also, Raman spectra of ices XV[24] and XIX[25] were reported. Since the pioneering IR spectroscopy studies on high-pressure ices by Whalley et al., more than 50 years have passed without any new spectra recorded. For none of the ices X−XIX discovered after the 1960s, spectra are available as of today neither in the far-, mid-, or near-infrared. Here, we provide near-infrared spectra of the six high-pressure polymorphs II, IV, V, VI, IX, and XII. These high-pressure ice phases differ in terms of density and the arrangement of oxygen atoms in the lattice. The increase of density compared to ice I_h is achieved through bending and compression of hydrogen bonds (ices II, IX), changes in the ring topology (ices V, XII), ring threading (ice IV), and interpenetration of two independent ice networks (ice VI). Thus, the choice of ice phases here allows us to see the impact of different hydrogen-bond patterns on the spectra of the ices. All spectra were recorded after recovery to ambient pressure under cryo-conditions (~77 K) to avoid backconversion to

Received: October 29, 2020
Revised: December 16, 2020

stable ice I_h. Ice I_h serves as a reference and represents the only crystalline H_2O ice that has already been studied in literature in the NIR spectral range.[26−28]

EXPERIMENTAL SECTION

Sample Preparation and X-Ray Diffraction (XRD) Characterization. High-pressure ices II, IV, V, VI, IX, and XII were prepared using a custom-made piston-cylinder setup described in former studies of the Innsbruck group.[29] In brief, 600 μL of ultrapure water in an indium container was loaded into the high-pressure cell and cooled to 77 K. Ices II, V, VI, and IX were prepared through isobaric heating of ice I_h at different pressures and from 77 K to different temperatures at different heating rates[18,30,31] (ice II: 0.3 GPa and 210 K at 2 K min^{-1}; ice V: 0.5 GPa and 250 K at 2 K min^{-1}; ice VI: 1.0 GPa and 255 K at >5 K min^{-1}; and ice IX: 0.5 GPa and 170 K at 3 K min^{-1}). Ices IV and XII were prepared through isobaric heating of unannealed high-density amorphous ice (uHDA)[32] at 0.8 GPa and 170 K at 0.4 K min^{-1} and 180 K at >25 K min^{-1}, respectively.[20,21] Afterward, all samples were quenched to 77 K and recovered at ambient pressure. Before recording NIR spectra, the high-pressure samples were characterized by X-ray powder diffraction (Cu Kα_1 radiation; diffractometer, Siemens D5000 or Bruker D8 Advance), see Figure S1.

Near-Infrared Spectroscopy. All of the spectra presented here were recorded at ambient pressure and liquid nitrogen temperature (~77 K). At these conditions, all of the ices are metastable with respect to ice I_h but can be kept indefinitely without the occurrence of any conversion. Ice III cannot be measured at 77 K because it converts to its hydrogen-ordered counterpart ice IX below 170 K.[33] Whalley and co-workers had devised a cryo-mulling technique and added isopentane to the ice samples to reduce the amount of ice in the optical path, enabling them to measure these ice samples in transmission geometry without black frequencies at the detector, that is, frequencies at which no transmitted light is detected.[34] By contrast, we here work on pure ice samples, without any mulling agent, and use a diffuse reflectance setup for the spectroscopic measurement. For spectroscopic characterization within the range of 10 000−4000 cm^{-1} (1−2.5 μm), a Büchi NIR Flex N-500 benchtop spectrometer in diffuse reflectance mode was utilized. The high-pressure ice samples were powdered using a mortar under liquid nitrogen and transferred to a precooled quartz cuvette. In total, a layer of about 1 mm thickness was found to be sufficient to produce spectra with good signal-to-noise ratios. An optical cryo-microscopy image of such a powder is shown in Figure S2. Typical single grain diameters range from 15 to 40 μm. In addition to the single grains, larger aggregates of up to 350 μm are seen in the image. Then, the cuvette filled with the powdered sample and liquid nitrogen was placed in the optical path of the spectrometer. Due to the short acquisition time of a few seconds, the ice samples could be held at 77 K at all times during the experiment, preventing any undesired transitions. For each high-pressure ice, at least three independently prepared samples were analyzed, yielding at least 20 cumulative spectra per ice polymorph. Ice I_h was measured as a reference. Each cumulative spectrum was recorded within 16 s and represents a sum of 32 single spectra at resolution 8 cm^{-1}. That is, every spectrum shown in Figure 1 represents an average of 640 or more single spectra.

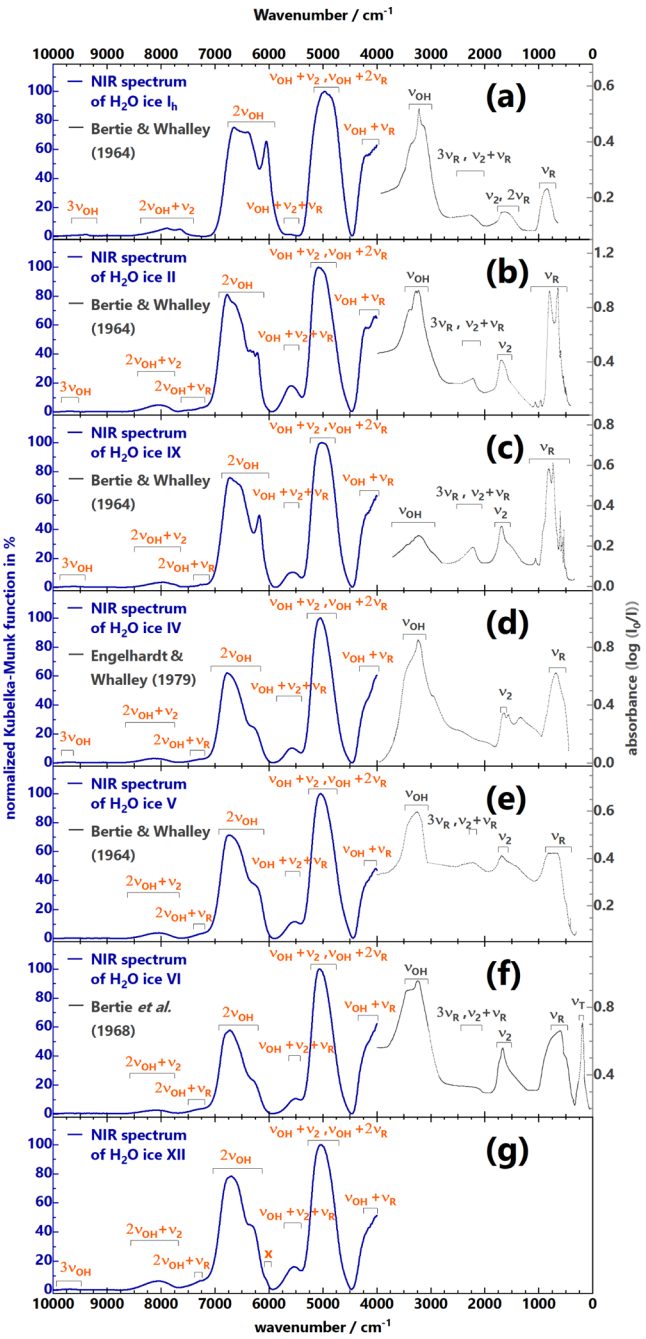

Figure 1. NIR spectra measured at ~77 K (in blue), together with MIR spectra recorded in the 1960s and 1970s by Whalley and co-workers at ~100 K from refs 14−16,35 (in gray). NIR spectra are normalized with respect to the band at ~5000 cm^{-1}. Band assignments are given, where "x" means "unassigned". Please note in (c) that Bertie and Whalley called the sample "ice III" even though it was measured at ~100 K, that is, below the ordering temperature to ice IX.

Conversion of Spectra. The reflectance spectra were converted to Kubelka−Munk (K−M) function spectra,[36,37] according to eq 1

$$F(R_\infty) = \frac{K}{S} = \frac{(1 - R_\infty)^2}{2R_\infty} \quad (1)$$

where $F(R_\infty)$ denotes the Kubelka−Munk or remission function, R_∞ is the reflectance of a layer sufficiently thick

https://dx.doi.org/10.1021/acs.jpca.0c09764
J. Phys. Chem. A XXXX, XXX, XXX−XXX

Table 1. Near-Infrared (NIR) Bands of Ice I_h Measured in Diffuse Reflectance in Comparison with the Data by Grundy and Schmitt[27,a]

peak position (cm^{-1})	peak position (μm)	assignment	Grundy and Schmitt[27] (cm^{-1})	deviation (cm^{-1})	deviation (μm)
9394	1.06	$3\nu_{OH}$	9586 ± 40	192	−0.021
7888	1.27	$2\nu_{OH} + \nu_2$	7847 ± 10	−41	0.007
7656	1.31		7628 ± 3	−28	0.005
			7256 ± 50		
6648	1.50	$2\nu_{OH}$	6682 ± 5	34	−0.008
			6579 ± 10		
6390	1.56		6403 ± 20	13	−0.003
			6319 ± 20		
6050	1.65		6055 ± 1	5	−0.001
5600	1.79	$\nu_{OH} + \nu_2 + \nu_R$	5565 ± 10	−35	0.011
4971	2.01	$\nu_{OH} + \nu_2$; $\nu_{OH} + 2\nu_R$	4983 ± 20	12	−0.005
4879	2.05		4948 ± 20	69	−0.029
4851	2.06		4837 ± 20	−14	0.006
4187	2.39	$\nu_{OH} + \nu_R$	4239 ± 5	52	−0.029
4145	2.41				
4107	2.43				
4066	2.46				
4034	2.48				
			3960 ± 5		

[a]Bands measured by G&S refer to a temperature of 80 K. Our bands were measured at 77 K.

that transmission is negligible, and K and S are the absorption and scattering coefficients of the sample, respectively. Then, a baseline correction was applied by subtracting a basis spline constructed from eight anchor points (local minima of the K−M function) from the raw spectra. An example of such a baseline correction is shown in Figure S3. These single spectra were then normalized to a characteristic band and summed up. Finally, the sum spectra were normalized to the corresponding (global) maximum of the K−M function. To identify peak centers, we have not used a Gaussian decomposition procedure but rather employed first and second derivative spectra. Peak centers of the K−M function were identified as the zero crossings of the first derivative. Shoulders were identified through minima in the first derivative and zero crossings in the second derivative (see Figure S4).

RESULTS AND DISCUSSION

Figure 1 shows a summary of our spectra in the NIR range, together with the mid-infrared (MIR) spectra recorded by Whalley and co-workers.[14−16,35] The plot shows six high-pressure ice polymorphs and ice I_h, as discussed individually below.

Ice I_h is the only crystalline ice for which several NIR spectra are available at different temperatures. Rajaram et al.[38] and Warren and Brandt[13] provide the most recent reviews on measurements of optical constants of ice, all of which were done on thin films in transmittance. Leto et al. compared amorphous ice films with crystalline ice films in the range 1.33−2.50 μm (7500−4000 cm^{-1}) at 16−150 K.[28] The most comprehensive work is reported by Grundy and Schmitt,[27] who report transmission spectra in the range 20−270 K in the spectral range also investigated by us. To disentangle overlapping spectral features, they fit a number of Gaussians to each absorption band. As a result, Grundy and Schmitt identified 15 absorptions from 1.04 to 2.53 μm (9586−3960 cm^{-1}). However, they rightly point out that some Gaussians may not correspond to real vibrational modes but may be artifacts resulting from the fitting method.[27] In the same spectral range, we also identify 15 absorptions in diffuse reflectance, as seen in Figure 1a and listed in Table 1. Most of the features identified by Grundy and Schmitt are also identified by us directly, with the exception of the bands at 7256 cm^{-1} (1.38 μm), 6579 cm^{-1} (1.52 μm), and 6319 cm^{-1} (1.58 μm). Furthermore, our spectral data exhibit more fine structure in the $\nu_{OH} + \nu_R$ region, that is, the combination band of the OH-stretching ν_{OH} and the libration ν_R mode. We here recognize five sub-bands at 4034−4187 cm^{-1} (2.48−2.39 μm), instead of just two.

Considering the $\nu_{OH} + 2\nu_R$ combination band between 4971 and 4851 cm^{-1}, our results agree well with the ones published by Grundy and Schmitt.[27] As pointed out by Ockman,[39] this range also contains the $\nu_{OH} + \nu_2$ combination band, where ν_2 represents the bending mode. Grundy and Schmitt assume the weak feature at 5600 cm^{-1} to be an artifact resulting from Gaussian decomposition, but we here assign it to combination band $\nu_{OH} + \nu_2 + \nu_R$. Comparing the strong and sharp low-frequency contribution to the first overtone $2\nu_{OH}$ at 6050 cm^{-1}, our result and the one of Grundy and Schmitt coincide within 5 cm^{-1}. In total, we recognize three sub-bands for $2\nu_{OH}$, 6050 cm^{-1} (1.65 μm), 6390 cm^{-1} (1.56 μm), and 6648 cm^{-1} (1.50 μm) (see Table 1). Above 7000 cm^{-1}, we identify three bands at 7656, 7888 cm^{-1}, and 9394 cm^{-1}, which represent combination $2\nu_{OH} + \nu_2$ and second overtone $3\nu_{OH}$.[39,40] That is, even at the upper and lower boundaries of the spectral range, all bands agree to better than 0.03 μm with the data by Grundy and Schmitt (see Table 1). This demonstrates that our

https://dx.doi.org/10.1021/acs.jpca.0c09764
J. Phys. Chem. A XXXX, XXX, XXX−XXX

procedure of defining the baseline and evaluating the Kubelka−Munk function (see Experimental Section) does not produce artifacts and that our spectra of powdered samples collected in diffuse reflectance mode compare in an excellent way with literature spectra obtained from thin films in transmission mode. One major advantage of the diffuse reflectance setup is that we do not need to worry about producing films of an appropriate thickness, suited for the absorptivities of the specific bands. Specifically, we do not need to make very thin samples for strong signals such as $2\nu_{OH}$ and very thick samples for weak signals such as $3\nu_{OH}$. Instead, we only need to make sure that enough powder is loaded to prevent the incoming beam from transmitting the sample. This testifies that the spectra reported in the following for high-pressure ice polymorphs represent reliable spectroscopic information.

For the high-pressure polymorphs, no NIR data are available so far, with the exceptions of ice VI and ice VII. Larsen and Williams scrutinized the overtone spectrum of stretching and bending vibrations in H_2O and D_2O up to pressures of 37 GPa at 300 K.[41] Kagi et al. investigated ices VI and VII as an inclusion in a cuboid diamond in the range of 4500−5500 cm^{-1}.[8] The identification of the ice NIR spectra in that study has proven to be difficult because of the spectroscopic signatures of the diamond itself and signatures from other inclusions, such as liquid water, masking the ice bands. By contrast, we here report the ice VI spectra of the pure substance at 77 K and ambient pressure (solely minor impurities of ice XII in ice IV could not be avoided—see Figure S1b). Figure 1b−g shows the spectra of six high-pressure polymorphs. All of them have quite different oxygen atom networks. Two belong to the trigonal crystal system, namely, ice II (space group *R*-3) and ice IV (*R*-3*c*); three are tetragonal, ice VI ($P42/nmc$), ice IX ($P4_12_12$), and ice XII ($I\text{-}42d$); and one is monoclinic, ice V ($C2/c$). The latter has 28 molecules in its unit cell, whereas hexagonal ice has only 4. The other five high-pressure polymorphs have 10 (ice VI), 12 (ices II, IX, XII), and 16 (ice IV) water molecules per unit cell. While ice II and ice IX feature hydrogen order, ices IV, V, VI, and XII are hydrogen-disordered. Table 2 summarizes the NIR bands for the high-pressure polymorphs identified in this work.

We are able to resolve eight different types of combination bands and overtones that are labeled in Table 2. In total, 24 individual bands can be identified for ices II and IX but only 16 or 17 for ices IV, V, and VI (see Table 2). This is not surprising since sharper features are expected for H-ordered ices II and IX than for H-disordered ices IV, V, and VI. However, H-disordered ice XII is an exception to the rule—it shows 25 bands. This is probably related to its complex O-atom network, involving only large seven- and eight-membered rings, whereas all other ices studied here feature smaller four-, five-, or six-membered rings.[42] In general, all high-pressure polymorphs show three intense features, just like hexagonal ice. These are $2\nu_{OH}$, $\nu_{OH} + \nu_2/\nu_{OH} + 2\nu_R$, and $\nu_{OH} + \nu_R$ and bands centered at about 6500, 5000, and 4100 cm^{-1}. In addition, the feature near 5500 cm^{-1} is much more pronounced in all spectra of high-pressure ices than in hexagonal ice. We tentatively assign this band to the $\nu_{OH}+\nu_2+\nu_R$ combination mode. We also identify weak second overtone $3\nu_{OH}$ but refrain from assigning it in ices V and VI because it is close to the noise level.

Figure 2a focuses on the $2\nu_{OH}$ band, which is the most suitable marker band to clearly distinguish all high-pressure

Table 2. Near-Infrared (NIR) Bands for High-Pressure Ices Measured in Diffuse Reflectance at 77 K

peak position (cm^{-1})					
ice II	ice IX	ice IV	ice V	ice VI	ice XII
		$3\nu_{OH}$			
9691	9657	9725			9690
		$2\nu_{OH} + \nu_2$			
8130	7974	8153	8083	8252	8058
8079	7785	8130	8043	8135	
8049	7726	8113		8088	
8006		8055		8034	
		$2\nu_{OH} + \nu_R$			
7534	7264	7346	7254	7352	7269
7404	7190	7250		7248	
7255					
		$2\nu_{OH}$			
6772	6724	6774	6746	6725	6768
6664	6690	6353	6716	6310	6740
6624	6648	6324	6648		6697
6346	6620	6296	6311		6659
6291	6562		6281		6628
6216	6180		6253		6365
					6351
					6325
		not assigned			
					6067
		$\nu_{OH} + \nu_2 + \nu_R$			
5579	5564	5572	5522	5506	5534
	5553			5488	5503
					5400
		$\nu_{OH} + \nu_2$, $\nu_{OH} + 2\nu_R$			
5079	5034	5050	5043	5071	5049
5043	5019				5026
4948	4990				4991
4921	4952				4940
		$\nu_{OH} + \nu_R$			
4209	4196	4176	4191	4178	4206
4180	4162	4116	4158	4154	4161
4131	4132	4028	4118	4135	4144
4051	4107		4075	4096	4099
4020	4068		4048	4048	4044
	4045		4019		4025

ices. Ice I_h exhibits a sharp feature at 1.65 μm (6050 cm^{-1}). It is used in remote sensing techniques to identify ice I_h in astrophysical environments[43] as well as a temperature probe[28] due to its strong temperature dependence.[27] At 77 K, it is a very prominent and rather intense feature only for ice I_h but appears as a shoulder for all H-disordered high-pressure ices (ices IV, V, VI, and XII) highlighted by diamonds in Figure 2a. In the case of H-ordered ice IX, this feature is also intense, and in the case of H-ordered ice II, this feature splits into three sharp subpeaks. These splittings can only be observed on the overtone of the OH-stretching mode but not on the fundamental vibration in the MIR of ice II (see Figure 1b). The doubling in frequencies in the first overtone compared to the fundamental vibration allows for a better separation of sub-bands, resolving features in the NIR that remain hidden in the MIR. For this reason, the NIR spectra presented here with their high signal-to-noise ratio and high resolution are better suited to distinguish between high-pressure polymorphs than the literature spectra in the MIR range. Yet another feature

https://dx.doi.org/10.1021/acs.jpca.0c09764
J. Phys. Chem. A XXXX, XXX, XXX−XXX

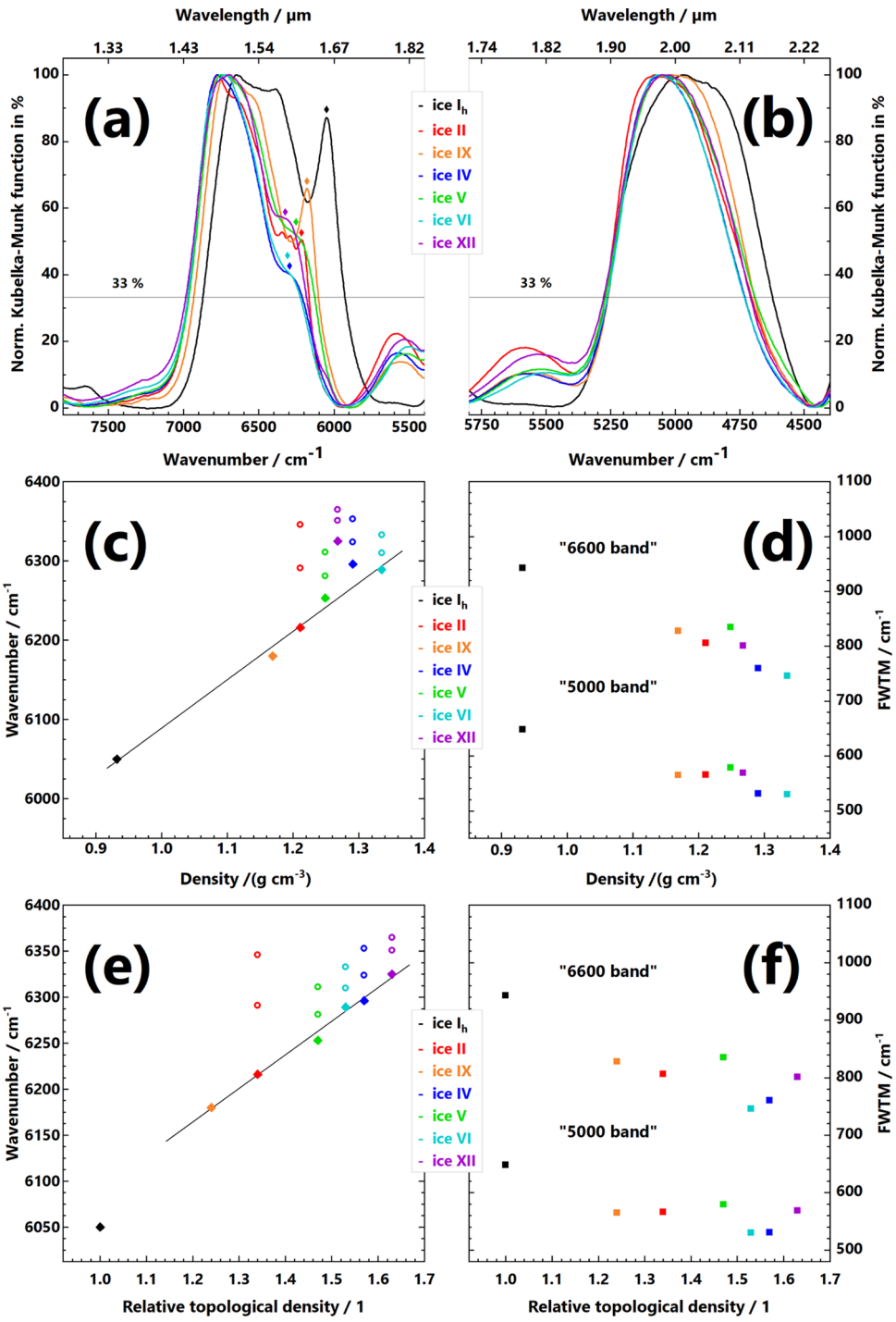

Figure 2. Comparison of the NIR features at (a) 6600 cm^{-1} and (b) 5000 cm^{-1}. (c–f) Correlation plots: (c) mass density and peak position, (d) mass density and full width at one-third of the maximum (FWTM), (e) topological density and peak position, and (f) topological density and FWTM. Filled diamonds in (c) and (e) correspond to the ones shown in (a). Open symbols in (c) and (e) represent sub-bands as extracted using the procedure shown in Figure S4.

that distinguishes all high-pressure ices from ice I_h is the $\nu_{OH} + \nu_2 + \nu_R$ wing centered near 5500 cm^{-1}. As seen in Figure 2b, this wing is only very weak in ice I_h but of medium intensity in all high-pressure ices.

It is immediately evident that all bands from high-pressure ices are blue-shifted compared to those from hexagonal ice (see Figure 2a,b). For example, the blue shift of the 6648 cm^{-1} band in ice I_h amounts to about +100 cm^{-1} for all ices, where ice IV is blue-shifted the most to 6774 cm^{-1}. Also, the 6050 cm^{-1} feature (1.65 μm) described above is blue-shifted between 130 cm^{-1} for ice IX and ~300 cm^{-1} for ice XII. The blue shift on this feature correlates quite well with the ambient pressure density of the ice polymorphs. Figure 2c shows a plot of the location of this feature versus the density of the high-pressure ice as determined by cryoflotation.[44] The trend is the denser the ice, the more blue-shifted the band, as indicated through the line guiding the eye in Figure 2c. Ice XII is an exception to this rule and shows the largest blue shift,

https://dx.doi.org/10.1021/acs.jpca.0c09764
J. Phys. Chem. A XXXX, XXX, XXX−XXX

even though ices IV and VI are slightly denser than ice XII. Figure 2e uses the topological density (relative to ice I_h) as defined by Herrero and Ramirez (Table 3 in ref 45). Although ices IV and XII have a lower density compared to ice VI, they show a higher topological density. This improves the correlation with NIR spectra greatly.

Significant differences between the high-pressure polymorphs can be noted when inspecting the full width at one-third of the maximum (FWTM) for the intense "6600 cm^{-1}" and "5000 cm^{-1}" bands (see Table 3 and Figure 2d,f).

Table 3. Full Width at One-Third of the Maximum (FWTM) of the $2\nu_{OH}$ and $\nu_{OH} + \nu_2/\nu_{OH} + 2\nu_R$ Bands

	$2\nu_{OH}$		$\nu_{OH} + \nu_2/\nu_{OH} + 2\nu_R$	
	band maximum (cm^{-1})	FWTM (cm^{-1})	band maximum (cm^{-1})	FWTM (cm^{-1})
ice I_h	6648	943	4971	648
ice II	6772	806	5079	566
ice IX	6724	828	5019	565
ice IV	6774	760	5050	531
ice V	6746	835	5043	579
ice VI	6725	746	5071	530
ice XII	6697	801	5049	569

Compared to ice I_h the FWTM is smaller for all high-pressure ices by up to 20%. Similar to the absolute position of the 6050 cm^{-1} feature, there is a weak correlation of the FWTM with density (Figure 2d)—the higher the density, the smaller the FWTM. In terms of topological density (Figure 2f), there is no clear correlation. Ice VI exhibits the narrowest bands, and ice I_h shows the broadest ones. The density correlation is, however, not strict. Ices V and XII exhibit broader bands than expected according to their density; ice V even shows broader bands than ices II and IX. This is possibly related to the H-ordered nature of the latter two and the H-disordered of the former. That is, to make a good correlation plot, not only density needs to be considered but also the H-order. This requires future work and more data on H-ordered ices, e.g., ices XIII, XIV, XV, and XIX.

CONCLUSIONS

In summary, we here report NIR spectra of six high-pressure ices ranging from densities of 1.16−1.34 g cm^{-3}, which is about 25−45% denser than ice I_h, the only ice polymorph for which NIR spectra have been available prior to our work. The increased density causes a strong blue shift of the overtones and combination bands compared to ice I_h. Also, the width of the bands is strongly reduced as the density increases. As a result, the sharp and strong feature useful to characterize ice I_h at 1.65 μm develops into a shoulder. Only for ices that are H-ordered, this sharp feature is retained, as in ice IX, or even split into several features, as in ice II. Yet, this band, the first overtone of the OH-stretching mode, is characteristic of these ices and can be used to identify the polymorphs. Tables 2 and 3 summarize the bands observed in our work, and Figure 1 compares our NIR spectra directly with MIR spectra obtained in pioneering works[14−17] (where ice XII is still lacking MIR data). Our attempts to extract anharmonicity from a comparison between the fundamental modes and the overtones/combination bands have been unsuccessful, especially because all of the bands are very broad, featuring severe coupling of modes and several subpeaks. Such attempts might be more successful for H-ordered ices, which are the focus of our ongoing work on NIR spectra of H_2O polymorphs. All spectra recorded in this work are also provided in the electronic form in the Supporting Material.

ASSOCIATED CONTENT

Supporting Information

The Supporting Information is available free of charge at https://pubs.acs.org/doi/10.1021/acs.jpca.0c09764.

Powder X-ray diffractograms of each high-pressure ice sample used in the present study; optical microscopy image of a powdered sample of hexagonal ice I_h at 248 K; depiction of the baseline correction procedure deployed; and peak identification based on first and second derivative spectra (PDF)

Normalized Kubelka−Munk function in % for ices I_h, II, IV, V, VI, IX, and XII is shown in Figures 1 and 2a,b (TXT)

Raw Kubelka−Munk function spectra of ice I_h (TXT)

Raw Kubelka−Munk function spectra of ice II (TXT)

Raw Kubelka−Munk function spectra of ice IV (TXT)

Raw Kubelka−Munk function spectra of ice V (TXT)

Raw Kubelka−Munk function spectra of ice VI (TXT)

Raw Kubelka−Munk function spectra of ice IX (TXT)

Raw Kubelka−Munk function spectra of ice XII (TXT)

AUTHOR INFORMATION

Corresponding Author

Thomas Loerting − *Institute of Physical Chemistry, University of Innsbruck, A-6020 Innsbruck, Austria;* orcid.org/0000-0001-6694-3843; Email: thomas.loerting@uibk.ac.at

Authors

Christina M. Tonauer − *Institute of Physical Chemistry, University of Innsbruck, A-6020 Innsbruck, Austria*

Eva-Maria Köck − *Institute of Physical Chemistry, University of Innsbruck, A-6020 Innsbruck, Austria; Max-Planck-Institut für Chemische Energiekonversion, D-45470 Mülheim an der Ruhr, Germany;* orcid.org/0000-0002-4642-8315

Tobias M. Gasser − *Institute of Physical Chemistry, University of Innsbruck, A-6020 Innsbruck, Austria*

Violeta Fuentes-Landete − *Institute of Physical Chemistry, University of Innsbruck, A-6020 Innsbruck, Austria; Max-Planck-Institut für Chemische Energiekonversion, D-45470 Mülheim an der Ruhr, Germany*

Raphael Henn − *Institute of Analytical Chemistry and Radiochemistry, University of Innsbruck, A-6020 Innsbruck, Austria*

Sophia Mayr − *Institute of Analytical Chemistry and Radiochemistry, University of Innsbruck, A-6020 Innsbruck, Austria*

Christian G. Kirchler − *Institute of Analytical Chemistry and Radiochemistry, University of Innsbruck, A-6020 Innsbruck, Austria*

Christian W. Huck − *Institute of Analytical Chemistry and Radiochemistry, University of Innsbruck, A-6020 Innsbruck, Austria;* orcid.org/0000-0002-6272-3242

Complete contact information is available at: https://pubs.acs.org/10.1021/acs.jpca.0c09764

Notes

The authors declare no competing financial interest.

https://dx.doi.org/10.1021/acs.jpca.0c09764
J. Phys. Chem. A XXXX, XXX, XXX−XXX

■ ACKNOWLEDGMENTS

The authors thank Astrid Hauptmann and Alexander Thoeny for experimental help. The authors are grateful to the Center for Molecular Water Sciences Hamburg (CMWS) and the Austrian Science Fund (FWF) for support under the bilateral grant I1392. V.F.-L. and E.-M.K. are grateful to the Max Planck Institute for Chemical Energy Conversion for the financial support, and C.M.T. is a recipient of a DOC fellowship of the Austrian Academy of Sciences ÖAW.

■ REFERENCES

(1) Tammann, G. The Connection of the Volume Surface to Polymorphism of Water. *Z. Phys. Chem.* **1913**, *84*, 293−312.
(2) Tammann, G. On the State Diagram of Water. *Z. Phys. Chem.* **1913**, *84*, 257−292.
(3) Tammann, G. The Behaviour of Water at High Pressure and Low Temperatures. *Z. Phys. Chem.* **1910**, *72*, 609−631.
(4) Tammann, G. Ice III. *Z. Anorg. Chem.* **1909**, *63*, 285−305.
(5) Bridgman, P. W. Verhalten des Wassers als Flüssigkeit und in fünf festen Formen unter Druck. *Anorg. Chem.* **1912**, *77*, 377−455.
(6) Engelhardt, H.; Whalley, E. Ice IV. *J. Chem. Phys.* **1972**, *56*, 2678−2684.
(7) Bridgman, P. W. The Pressure-Volume-Temperature Relations of the Liquid, and the Phase Diagram of Heavy Water. *J. Chem. Phys.* **1935**, *3*, 597−605.
(8) Kagi, H.; Lu, R.; Davidson, P.; Goncharov, A. F.; Mao, H. K.; Hemley, R. J. Evidence for Ice VI as an Inclusion in Cuboid Diamonds from High P-T Near Infrared Spectroscopy. *Mineral. Mag.* **2000**, *64*, 1089−1097.
(9) Tschauner, O.; Huang, S.; Greenberg, E.; Prakapenka, V. B.; Ma, C.; Rossman, G. R.; Shen, A. H.; Zhang, D.; Newville, M.; Lanzirotti, A. Ice-VII Inclusions in Diamonds: Evidence for Aqueous Fluid in Earth's Deep Mantle. *Science* **2018**, *359*, 1136−1139.
(10) Smit, K. V.; Shirey, S. B. Diamonds Help Solve the Enigma of Earth's Deep Water. *Gems Gemol.* **2018**, *54*, 220−223.
(11) Consolmagno, G. J. Ice-Rich Moons and the Physical Properties of Ice. *J. Phys. Chem. A* **1983**, *87*, 4204−4208.
(12) Warren, S. G. Optical Constants of Ice from the Ultraviolet to the Microwave. *Appl. Opt.* **1984**, *23*, 1206−1225.
(13) Warren, S. G.; Brandt, R. E. Optical Constants of Ice from the Ultraviolet to the Microwave: A Revised Compilation. *J. Geophys. Res.* **2008**, *113*, No. D14220.
(14) Bertie, J. E.; Whalley, E. Infrared Spectra of Ices II, III, and V in the Range 4000 to 350 cm^{-1}. *J. Chem. Phys.* **1964**, *40*, 1646−1659.
(15) Engelhardt, H.; Whalley, E. The Infrared Spectrum of Ice IV in the Range 4000-400 cm^{-1}. *J. Chem. Phys.* **1979**, *71*, 4050−4051.
(16) Bertie, J. E.; Labbe, H. J.; Whalley, E. Infrared Spectrum of Ice VI in the Range 4000 - 50 cm^{-1}. *J. Chem. Phys.* **1968**, *49*, 2141−2144.
(17) Bertie, J. E.; Labbe, H. J.; Whalley, E. Far-Infrared Spectra of Ice II, V and IX. *J. Chem. Phys.* **1968**, *49*, 775−780.
(18) Minčeva-Šukarova, B.; Sherman, W. F.; Wilkinson, G. R. A High-Pressure Spectroscopic Study of the Ice III - Ice IX, Disordered - Ordered Transition. *J. Mol. Struct.* **1984**, *115*, 137−140.
(19) Minčeva-Šukarova, B.; Sherman, W. F.; Wilkinson, G. R. The Raman Spectra of Ice (I_h, II, III, V, VI and IX) as Functions of Pressure and Temperature. *J. Phys. C: Solid State Phys.* **1984**, *17*, 5833−5850.
(20) Salzmann, C. G.; Kohl, I.; Loerting, T.; Mayer, E.; Hallbrucker, A. Raman Spectroscopic Study on Hydrogen Bonding in Recovered Ice IV. *J. Phys. Chem. B* **2003**, *107*, 2802−2807.
(21) Salzmann, C.; Kohl, I.; Loerting, T.; Mayer, E.; Hallbrucker, A. The Raman Spectrum of Ice XII and Its Relation to That of a New "High-Pressure Phase of H_2O Ice". *J. Phys. Chem. B* **2002**, *106*, 1−6.
(22) Salzmann, C. G.; Hallbrucker, A.; Finney, J. L.; Mayer, E. Raman Spectroscopic Features of Hydrogen-Ordering in Ice XII. *Chem. Phys. Lett.* **2006**, *429*, 469−473.
(23) Salzmann, C. G.; Hallbrucker, A.; Finney, J. L.; Mayer, E. Raman Spectroscopic Study of Hydrogen Ordered Ice XIII and of Its Reversible Phase Transition to Disordered Ice V. *Phys. Chem. Chem. Phys.* **2006**, *8*, 3088−3093.
(24) Whale, T. F.; Clark, S. J.; Finney, J. L.; Salzmann, C. G. DFT-Assisted Interpretation of the Raman Spectra of Hydrogen-Ordered Ice XV. *J. Raman Spectrosc.* **2013**, *44*, 290−298.
(25) Thoeny, A. V.; Gasser, T. M.; Loerting, T. Distinguishing Ice β-XV from Deep Glassy Ice VI: Raman Spectroscopy. *Phys. Chem. Chem. Phys.* **2019**, *21*, 15452−15462.
(26) Clark, R. N. Water Frost and Ice - the Near Infrared Spectral Reflectance at 0.65−2.5 μm. *J. Geophys. Res.* **1981**, *86*, 3087−3096.
(27) Grundy, W. M.; Schmitt, B. The Temperature-Dependent Near-Infrared Absorption Spectrum of Hexagonal H_2O Ice. *J. Geophys. Res.* **1998**, *103*, 25809−25822.
(28) Leto, G.; Gomis, O.; Strazzulla, G. The Reflectance Spectrum of Water Ice: Is the 1.65 μm Peak a Good Temperature Probe? *Mem. Soc. Astron. Ital. Suppl.* **2005**, *6*, 57−62.
(29) Tonauer, C. M.; Seidl-Nigsch, M.; Loerting, T. High-Density Amorphous Ice: Nucleation of Nanosized Low-Density Amorphous Ice. *J. Phys.: Condens. Matter* **2018**, *30*, No. 034002.
(30) Mishima, O.; Endo, S. Phase Relations of Ice under Pressure. *J. Chem. Phys.* **1980**, *73*, 2454−2456.
(31) Shephard, J. J.; Salzmann, C. G. The Complex Kinetics of the Ice VI to Ice XV Hydrogen Ordering Phase Transition. *Chem. Phys. Lett.* **2015**, *637*, 63−66.
(32) Mishima, O.; Calvert, L. D.; Whalley, E. "Melting Ice" I at 77 K and 10 kbar: A New Method of Making Amorphous Solids. *Nature* **1984**, *310*, 393−395.
(33) Petrenko, V. F.; Whitworth, R. W. *Physics of Ice*; Oxford University Press: Oxford, 1999.
(34) Bertie, J. E.; Whalley, E. Infrared Spectra by Mulling Techniques at Liquid Nitrogen Temperatures. *Spectrochim. Acta* **1964**, *20*, 1349−1356.
(35) Bertie, J. E.; Whalley, E. Infrared Spectra of Ices I_h and I_c in the Range 4000 to 350 cm^{-1}. *J. Chem. Phys.* **1964**, *40*, 1637−1645.
(36) Kubelka, P.; Munk, F. An Article on Optics of Paint Layers. *Fuer Tekn. Phys.* **1931**, *12*, 593−609.
(37) Torrent, J.; Barron, V. *Diffuse Reflectance Spectroscopy*; American Society of Agronomy and Soil Science: Madison, WI, 2015.
(38) Rajaram, B.; Glandorf, D. L.; Curtis, D. B.; Tolbert, M. A.; Toon, O. B.; Ockman, N. Temperature-Dependent Optical Constants of Water Ice in the near Infrared: New Results and Critical Review of the Available Measurements. *Appl. Opt.* **2001**, *40*, 4449−4462.
(39) Ockman, N. The Infrared and Raman Spectra of Ice. *Adv. Phys.* **1958**, *7*, 199−220.
(40) Ockman, N.; Sutherland, G. B. B. M. Infrared and Raman Spectra of Single Crystals of Ice. *Proc. R. Soc. London* **1958**, *247*, 434−440.
(41) Larsen, C. F.; Williams, Q. Overtone Spectra and Hydrogen Potential of H_2O at High Pressure. *Phys. Rev. B* **1998**, *58*, 8306−8312.
(42) Salzmann, C. G.; Radaelli, P. G.; Slater, B.; Finney, J. L. The Polymorphism of Ice: Five Unresolved Questions. *Phys. Chem. Chem. Phys.* **2011**, *13*, 18468−18480.
(43) Grundy, W. M.; Buie, M. W.; Stansberry, J. A.; Spencer, J. R.; Schmitt, B. Near-Infrared Spectra of Icy Outer Solar System Surfaces: Remote Determination of H_2O Ice Temperatures. *Icarus* **1999**, *142*, 536−549.
(44) Loerting, T.; Bauer, M.; Kohl, I.; Watschinger, K.; Winkel, K.; Mayer, E. Cryoflotation: Densities of Amorphous and Crystalline Ices. *J. Phys. Chem. B* **2011**, *115*, 14167−14175.
(45) Herrero, C. P.; Ramirez, R. Topological Characterization of Crystalline Ice Structures from Coordination Sequences. *Phys. Chem. Chem. Phys.* **2013**, *15*, 16676−16685.

https://dx.doi.org/10.1021/acs.jpca.0c09764
J. Phys. Chem. A XXXX, XXX, XXX−XXX